# Interannual modulation of extratropical high frequency variability

**Rodrigo Caballero**
*Dipartimento di Fisica, Università di Roma «La Sapienza», Roma, Italy*

**Abstract**
A simple explanation is presented for the observed interannual changes in the dominant space and time scales of Northern Hemisphere winter extratropical high frequency variability. It is found that such changes can successfully be predicted by linearizing a 2-level quasi-geostrophic model in spherical geometry around the observed zonal mean states. The mechanisms responsible for the selection of the most unstable normal mode are investigated.

**Key words** *tropical-extratropical interactions – baroclinic instability – most unstable normal mode*

## 1. Introduction

The study of tropical-extratropical interactions in the atmosphere has in the past focused mainly on issues such as teleconnection processes and barotropic Rossby wave propagation. Less attention been paid to the high frequency component of the motion.

Recently, detailed study of the statistics of transient eddies has revealed some interesting features. In a GCM study, Mechoso *et al.* (1987) computed the space-time power spectrum of their model's extratropical variability. They separated eastward-, westward- and non-propagating contributions using Hayashi's (1971) technique, and found that when their model was forced with the climatological Sea Surface Temperature (SST) field, the eastward-propagating spectrum had a single peak at zonal wavenumber 4 with a period of around 10 days. When an El Niño-like anomaly was added to the climatological SST, the peak became stronger and shifted to wavenumber 6 with a period of around 4 days.

Similar behaviour was found in an observational study by Hansen *et al.* (1989). The study used 16 years of Northern Hemisphere winter data. Individual winters were classified as El Niño, anti-El Niño and «control» (*i.e.*, neither El Niño nor anti-El Niño) and Hayashi spectra were computed and averaged over each class. The eastward-propagating spectra of the anti-El Niño and control composites both showed a dominant peak at zonal wavenumber 5 with around a 9 day period. In the El Niño composite the peak was at wavenumber 7 with around a 5 day period, and had higher amplitude than in the control composite.

In this note we propose a simple linear explanation for the observed changes in the spectral peak. The model and results are presented in section 2; section 3 investigates the mechanisms that may preside over the selection of the preferred space and time scales, and in section 4 we discuss our results.

*Mailing address*: Dr. Rodrigo Caballero, Dipartimento di Fisica, Università di Roma «La Sapienza», P.le A. Moro 5, 00185 Roma, Italy; e-mail: caballero@roma1.infn.it

*Current affiliation*: Department of Geophysics, NBI f AFG, University of Copenhagen, Juliane Maries Vej 30, DK-2100 Copenhagen Ø, Denmark.

## 2. Model and results

Since the pioneering work of Charney (1947) and Eady (1949), the eastward-propagating long waves in midlatitudes have been associated with the baroclinic instability of the zonal mean westerlies. These propagating waves present themselves as a turbulent (or at least chaotic) mixture of eddies of various space and time scales. It may reasonably be supposed that the dominant peak in the space-time spectrum of the eddies corresponds to the space and time scale at which energy is injected into the system. Within the framework of the linear instability theory, energy is transferred from the mean flow to the eddies predominantly through the Most Unstable Normal Mode (MUNM). We shall follow tradition by assuming that: 1) the relevant basic state for linear instability calculations is the time and zonal mean state; 2) the zonal wavenumber and period of the spectral peak correspond to those of the MUNM. We shall further assume that higher growth rates of the MUNM imply greater variability and hence a stronger spectral peak. We note however that the validity of these assumptions has never been rigorously demonstrated, so they have a purely heuristic value.

Under the above assumptions, we may go about explaining interannual variations in the position and amplitude of the spectral peak by studying changes in the time and zonal mean state and its associated MUNM. Our procedure will be to linearize the equations of motion around observed basic states obtained by averaging over El Niño, anti-El Niño and control winters in a manner analogous to that described in section 1 and computing the MUNM in each case.

### 2.1. *Equations*

We shall use the two-level inviscid quasi-geostrophic system in the standard formulation of Pedlosky (1979):

$$\partial_t q_i + J(\psi_i, q_i) = 0 \qquad i = 1,2$$

where

$$q_i = \Delta\psi_i + f + (-1)^i F(\psi_1 - \psi_2),$$

subscripts 1 and 2 referring to the upper and lower levels respectively. $F$ is the Froude number. Full sphericity is retained in the spatial derivatives and in the Coriolis parameter $f = 2\Omega \sin\varphi$, where $\varphi$ is latitude. Other symbols have their usual meteorological meaning.

We write the streamfunction as the sum of a time and zonal average and a small perturbation:

$$\psi_i(\lambda, \varphi, t) = -\int_{\varphi_0}^{\varphi} U_i(\varphi')\, a\, d\varphi' + \psi_i'(\lambda, \varphi, t)$$

where $U_i(\varphi)$ is the zonal wind averaged over time $t$ and longitude $\lambda$, and $a$ is the Earth's radius. Substituting into the equations of motion and neglecting second order terms, we obtain:

$$\partial_t q_i' + \frac{U_i(\varphi)}{a\cos\varphi}\partial_\lambda q_i' + \frac{\Pi_i(\varphi)}{a\cos\varphi}\partial_\lambda \psi_i' = 0 \quad (2.1)$$

where

$$q_i' = \Delta\psi_i' + (-1)^i F(\psi_1' - \psi_2')$$

and

$$\Pi_i(\varphi) = \frac{1}{4}\frac{d}{d\varphi}f - \frac{1}{a^2}$$

$$\left(\frac{d^2}{d\varphi^2} - \tan\varphi\frac{d}{d\varphi} - \frac{1}{\cos^2\varphi}\right)U_i - (-1)^i F(U_1 - U_2).$$

We must solve (2.1) for $\psi_i'$. The equations contain time and longitude only through partial derivatives and so we may expect the dependence of solutions on these variables to be of the form $e^{i(m\lambda - \omega t)}$, where $m$ is a zonal wavenumber and $\omega$ is the frequency. The presence of meridional shear in the zonal mean wind, however, makes the equations non separable. Thus we expect solutions of the form

$$\psi_i' = A_i(\varphi)\, e^{i(m\lambda - \omega t)} + \text{c.c.}$$

where c.c. indicates the complex conjugate of the preceding expression and $A_i(\varphi)$ is some complex, latitudinally varying amplitude. Sub-

stituting this form into (2.1) and fixing $m$, we obtain an eigenvalue problem for $\omega$ and its associated eigenvector $A_{i\omega}(\varphi)$:

$$\left(\omega - m\frac{U_i(\varphi)}{a\cos\varphi}\right)\left(\frac{1}{a^2\cos\varphi}\partial_\varphi(\cos\varphi\,\partial_\varphi A_{i_\omega}) + \right.$$

$$\left. -\frac{m^2}{a^2\cos\varphi}A_{i_\omega} + (-1)^i F(A_{1_\omega} - A_{2_\omega})\right) + \quad (2.2)$$

$$-m\frac{\Pi_i(\varphi)}{a\cos\varphi}A_{i_\omega} = 0,$$

with appropriate boundary conditions.

Solutions $A_{i\omega}(\varphi)e^{i(m\lambda-\omega t)}$ + c.c. are referred to as normal modes. Frequencies $\omega$ will in general be complex. The mode with the highest $\mathrm{Im}(\omega)$ will be our Most Unstable Normal Mode (MUNM). We search for the MUNM by solving (2.2) numerically using a finite-difference scheme.

## 2.2. *Basic states*

A basic state may be prescribed by fixing zonal mean wind profiles for the upper and lower levels of the model. We use wind profiles taken from observations. Specifically, we used global analyzed ECMWF data for 8 Northern Hemisphere winters (1985/1986-1993/1994; winters defined as the 90 days from 1st December to 28th February). Using the Japan Meteorological Agency (1991) index, we thus have 3 El Niño winters (86/87, 87/88, 91/92), one anti-El Niño (88/89) and 4 which are neither («control»). We fix El Niño, anti-El Niño and control basic states by averaging the zonal mean winds over each of the three classes, taking 300 mb values for the upper level and 850 mb values for the lower level. The profiles are shown in fig. 1a (Northern Hemisphere only). The data were provided on a Gaussian grid with 48 latitude points and were linearly interpolated onto the regular grid used to solve the equations.

As an independent test, we also used NMC analysis data for the 20 winters from 1961/1962 to 1980/1981. Again using the JMA index, we now have 5 El Niños (63/64, 65/66, 69/70, 72/73, 76/77), 6 anti-El Niños (64/65, 67/68, 70/71, 71/72, 73/74, 75/76) and 9 control cases. This data set, though much longer than the ECMWF data set, has the shortcoming that it only provides 500 mb geopotential height data and only covers the region between 20°N and 85°N. We determined the zonal mean wind geostrophically through the approximation $\psi = gZ/f_0$, where $\psi$ is streamfunction, $Z$ is geopotential height, $g$ is the acceleration of gravity and $f_0$ is the Coriolis parameter evaluated at 45°N. The wind profile obtained from the meridional derivative of this streamfunction was assigned to the upper level, and the wind in the lower layer was set to zero. The resulting 500 mb wind profiles are shown in fig. 1b. Note that the use of 500 mb data leads to a severe underestimation of the mean angular velocity of the atmosphere, so that we cannot expect to obtain eigenmodes with realistic phase speeds. The results obtained are nonetheless of interest, as will be detailed in section 3.

## 2.3. *Results*

Preliminary investigation using the ECMWF profiles in a 2-level model of global extent showed the MUNMs always have maximum amplitude in the Northern Hemisphere extratropics, with a small secondary maximum in the Southern Hemisphere extratropics and negligible values in the tropics. Using a hemispheric (Northern Hemisphere) version of the model and prescribing zero perturbation amplitudes at Equator and Pole, the zonal wavenumber and frequencies of the MUNMs obtained were almost identical to those in the global model. Only the hemispheric results will be presented. In the NMC case, the extent of the model was further reduced to the channel between 25° and 80°N, and perturbation amplitudes were set to zero at channel boundaries. Biharmonic smoothing with a damping rate of 86 days was used. The only remaining free parameter in the equations is the Froude number, and the normal modes were computed for various values of this parameter.

Zonal wavenumbers, periods $2\pi/\mathrm{Re}(\omega)$ and e-folding times $1/\mathrm{Im}(\omega)$ for the MUNMs are shown in table Ia,b. The second most unstable

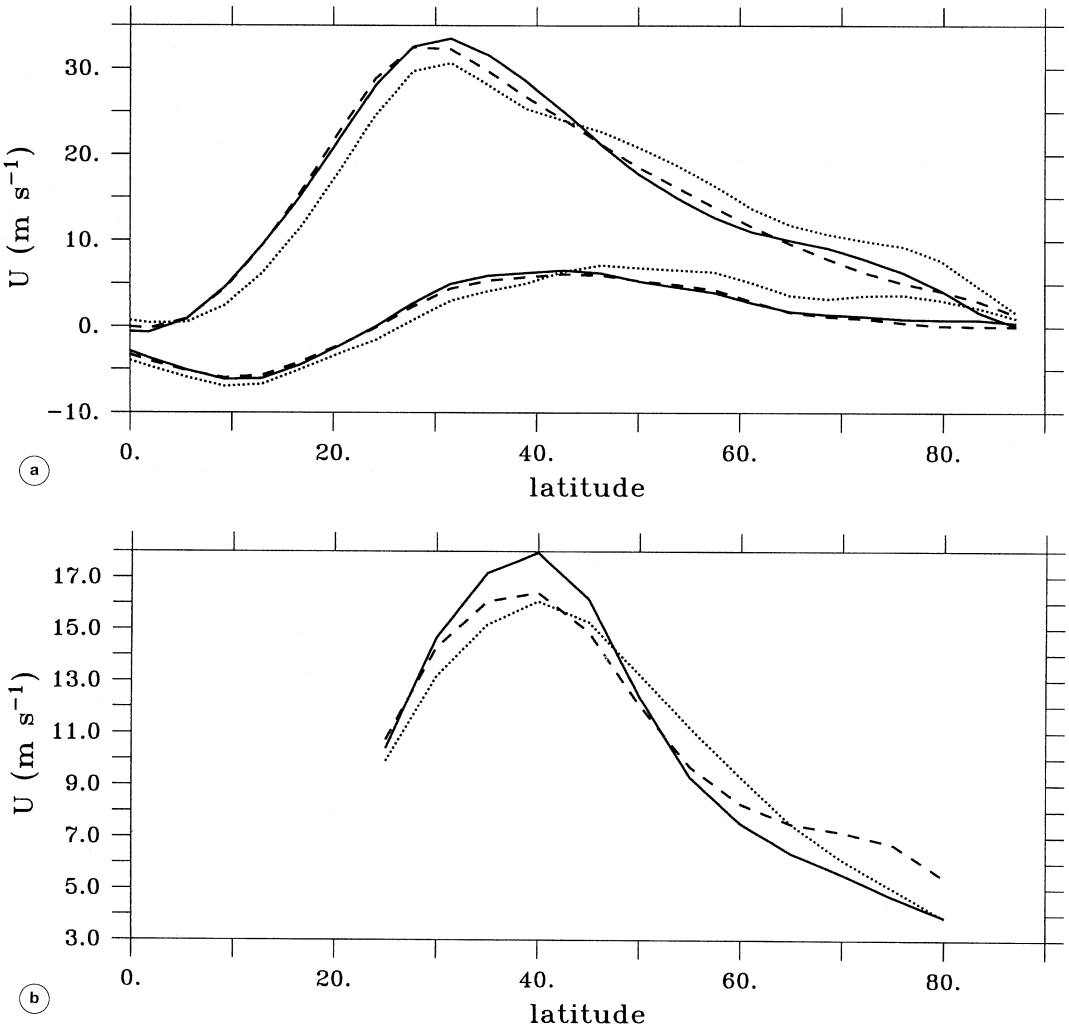


**Fig. 1a,b.** Zonal mean wind profiles used as basic states. a) ECMWF data at 300 mb (upper lines) and 850 mb (lower lines). b) NMC 500 mb wind computed geostrophically from the geopotential height (see text). Solid lines: averages over El Niño winters; dashed lines: averages over control winters; dotted lines: averages over anti-El Niño winters.

modes had e-folding times at least 50% longer than the MUNM's and will not be discussed.

Table Ia (ECMWF profiles) clearly shows the shift towards shorter time and space scales as we pass from anti-El Niño to El Niño profiles. The phenomenon is robust to variations in the Froude number. For $F = 2$, we even obtain quantitatively good agreement with the observational results of Hansen *et al.* (1989) (see section 1). The results for the NMC profiles (table Ib) show the same qualitative trend towards shorter scales during El Niño years, though the periods are unrealistically long (as could be expected from the discussion in section 2.2).

## 3. Scale selection

The complicated structure of (2.2) makes it difficult to establish analytically which features of a given profile determine the time and space scales of the MUNM. Some insight may however be gained by comparing table Ia,b and noting that the zonal wavenumbers of the MUNMs for El Niño, control and anti-El Niño profiles correspond fairly closely, while the periods and e-folding times are markedly longer in the NMC case. Examination of fig. 1a,b on the other hand, reveals that the three ECMWF profiles have *shapes* that are reasonably similar to the corresponding profiles in the NMC data, but the maximum values achieved by the *mean speed* and the *vertical shear* are much smaller in the latter (this of course is due to the fact that the NMC profiles correspond to 500 mb winds as opposed to 300 mb in the ECMWF case). This suggests that the spatial structure of the MUNM may be determined predominantly by the shape of the zonal wind profile, while the time scales are fixed mainly by the mean speed and vertical shear.

**Table Ia,b.** Zonal wavenumber, period and e-folding times of the MUNMs obtained with the El Niño, control and anti-El Niño basic states shown in fig. 1a,b.

| | El Niño | Control | Anti-El Niño |
|---|---|---|---|
| **a) ECMWF profiles** | | | |
| ***F* = 1.5** | | | |
| Wavenumber | 6 | 5 | 5 |
| Period (days) | 6.9 | 9.3 | 8.9 |
| e-folding time (days) | 6.0 | 5.9 | 11.7 |
| ***F* = 2.0** | | | |
| Wavenumber | 7 | 6 | 5 |
| Period (days) | 4.5 | 5.7 | 7.1 |
| e-folding time (days) | 2.9 | 2.9 | 4.0 |
| ***F* = 2.5** | | | |
| Wavenumber | 7 | 7 | 6 |
| Period (days) | 4.8 | 5.0 | 6.0 |
| e-folding time (days) | 2.1 | 2.2 | 2.9 |
| ***F* = 3.0** | | | |
| Wavenumber | 9 | 8 | 6 |
| Period (days) | 3.3 | 4.1 | 5.9 |
| e-folding time (days) | 1.6 | 1.7 | 2.4 |
| **b) NMC profiles** | | | |
| ***F* = 2** | | | |
| Wavenumber | 7 | 7 | 5 |
| Period (days) | 19.5 | 24.5 | 27.3 |
| e-folding time (days) | 3.5 | 3.7 | 4.4 |

A simple test of this hypothesis is to assign a profile and observe the changes in the MUNM as the shape, maximum mean speed and maximum vertical shear are varied independently. We shall use «jet-like» profiles of the form

$$P(\varphi, \varepsilon) = \frac{1}{N(\varepsilon)} [\sin(2\varphi) + \varepsilon \sin(4\varphi)]$$

where $\varepsilon$ is a variable parameter and $N(\varepsilon)$ is a normalization constant which keeps the maximum value of $P(\varphi, \varepsilon)$ at unit value as $\varepsilon$ is varied. As $\varepsilon$ grows, the jet narrows and moves southwards (fig. 2), as observed during El Niño events (fig. 1a,b). We define upper and lower level profiles as

$$U_1(\varphi) = (u+m)\, P(\varphi, \varepsilon)$$

$$U_2(\varphi) = (u-m)\, P(\varphi, \varepsilon)$$

so that we may vary the maximum mean speed through $u$, the maximum vertical shear through $m$ and the shape through $\varepsilon$. Three cases are considered:

a) $u = m = 15$ ms$^{-1}$ variable;
b) $\varepsilon = .3$, $m = 15$ ms$^{-1}$, $u$ variable;
c) $\varepsilon = .3$, $u = 15$ ms$^{-1}$, $m$ variable.

Results are summarized in table IIa-c. Overall, they may be said to corroborate our hypothesis.

In particular, table IIa shows a clear trend towards higher wavenumbers as the jet becomes more «El Niño-like», although this trend is far from smooth. The time scales do not vary appreciably, consistently with our hypothesis. Further, table IIb shows that the period of the MUNM responds strongly to changes in the maximum mean speed $u$, while the e-folding time shows a much weaker response. Note that the change in the period (*i.e.*, in the phase velocity of the mode) cannot be explained simply through the Galilean invariance of the system: because we are changing the mean speed through a multiplicative constant, the changes are not equivalent to changes of reference frame.

Much stronger variations in the e-folding time are obtained by changing the maximum vertical shear, as is shown by table IIc. Using an argument of the type originally proposed by

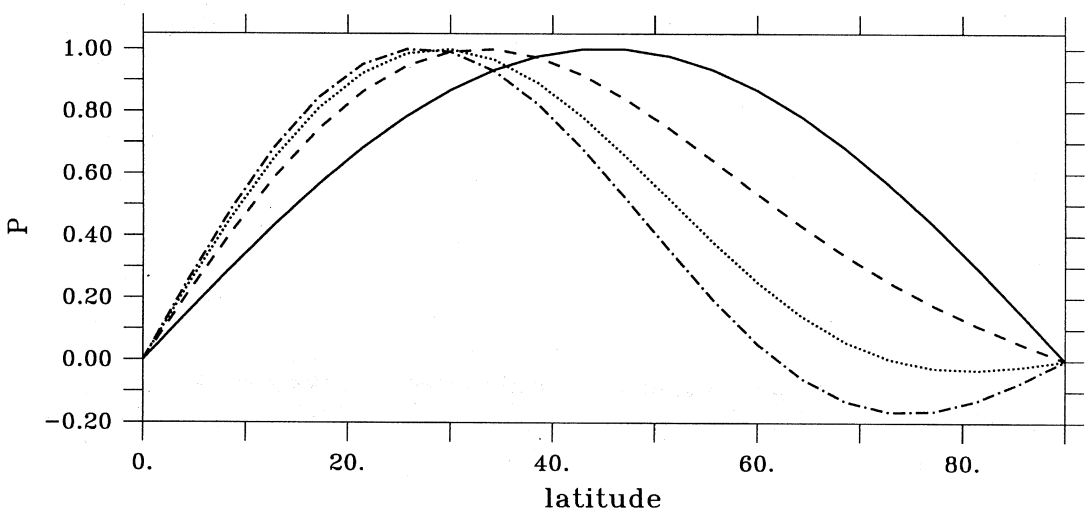


**Fig. 2.** The normalized profile $P(\varphi, \varepsilon)$ used to study the effects of changes in shape, shown at various values of $\varepsilon$: $\varepsilon = 0.0$ (solid line); $\varepsilon = 0.3$ (dashed); $\varepsilon = 0.6$ (dotted); $\varepsilon = 0.9$ (dot-dashed).

**Table IIa-c.** Variation of the space and time scales of the MUNMs as the shape, mean speed and vertical shear of the basic state are varied independently. a) Variation of shape (see fig. 2). $u = m = 15$ ms$^{-1}$; b) Variation of the mean speed; $\varepsilon = .3$, $m = 15$ ms$^{-1}$; c) Variation of the vertical shear; $\varepsilon = .3$, $u = 15$ ms$^{-1}$.

**a)**

| $\varepsilon$ | 0.0 | 0.3 | 0.6 | 0.9 |
|---|---|---|---|---|
| Wavenumber | 5 | 7 | 7 | 8 |
| Period (days) | 5.4 | 5.6 | 6.8 | 6.3 |
| e-folding time (days) | 1.5 | 1.3 | 1.3 | 1.3 |

**b)**

| $u$ (ms$^{-1}$) | 10 | 15 | 25 |
|---|---|---|---|
| Wavenumber | 7 | 7 | 7 |
| Period (days) | 13.4 | 5.6 | 2.6 |
| e-folding time (days) | 1.3 | 1.3 | 1.4 |

**c)**

| $m$ (ms$^{-1}$) | 10 | 15 | 25 |
|---|---|---|---|
| Wavenumber | 7 | 7 | 7 |
| Period (days) | 5.2 | 5.6 | 6.2 |
| e-folding time (days) | 2.6 | 1.3 | .7 |

Eady (1949), we can see how the e-folding time may change while the spatial structure of the mode remains relatively unmodified. Consider a baroclinic basic state with uniform vertical shear in which potential temperature surfaces make an angle $\beta$ with the horizontal. Consider furthermore an air parcel that is adiabatically displaced in the positive meridional and vertical direction, its trajectory making an angle $\alpha < \beta$ with the horizontal. It may be shown (Pedlosky 1979, p. 453) that the acceleration of the displaced particle is given by

$$N^2 \sin\alpha \, (\tan\beta - \tan\alpha) \, \delta y$$

where $N$ is the Brunt-Väisäla frequency and $\delta y$ is the horizontal displacement. Clearly, the acceleration grows with $\beta$, which amounts to saying that the e-folding time of a disturbance of fixed structure (fixed $\alpha$) decreases with increasing vertical shear of the zonal wind.

## 4. Summary and discussion

We have shown that the observed shift in the spectral peak of the eastward propagating variability towards shorter space and time scales during El Niño events may be explained rather well in the context of the «classical» baroclinic instability theory. During an El Niño winter, the zonal mean jet becomes sharper, more intense and moves slightly southward. This behaviour is consistent with simple models of the Hadley circulation such as those of Schneider and Lindzen (1977) and Held and

Hou (1980). In these models, an increase in tropical heating leads to stronger Hadley circulation, resulting in increased northward transport of zonal angular momentum at upper levels that leads to changes in the zonal mean wind similar to those observed during El Niño events.

The modification of the zonal mean state is reflected in the MUNMs. In particular, it appears that the change in shape of the mean zonal wind profile leads to higher zonal wavenumbers, while the increase in mean speed and vertical shear lead to higher phase velocity and growth rate.

Finally, we note that the results depend crucially on two assumptions (see section 2) whose validity is far from obvious. Gall (1976), using a multilevel primitive equation model and observed zonal mean states, found that the MUNMs typically had zonal wavenumbers of around 15. These, however, were very shallow modes, and they are inconsistent with the observed fact that transient eddies statistically have peak amplitudes in the upper troposphere. It may be that Gall's MUNMs are quickly damped by surface friction and reach smaller amplitudes than the slower growing but less damped eddies of longer wavelength, which have peak amplitude at upper levels. Our crude two level model would only capture these latter modes.

Further, Speranza and Malguzzi (1988) have questioned the correctness of identifying the time mean state with a fixed point of the equations of motion, since baroclinic instability is intrinsically asymmetric and the fluctuations induced in the zonal mean flow will not be distributed evenly about the zonally symmetric fixed point. They also contend that the chaotic nature of the extratropical circulation could arise from the instability or a more complex structure than a fixed point (*i.e.*, a limit cycle or torus). The consistency of our findings with these remarks requires careful study of the non-linear dynamics of the perturbations. This will be the subject of future work.

## Acknowledgements

I am indebted to Prof. A. Sutera for his continuing support and encouragement. I also thank Prof. A. Speranza for stimulating discussion. The comments of two anonymous reviewers improved the text. Computer support is acknowledged from CINECA under the ICARUS Programme.

*REFERENCES*

CHARNEY, J.G. (1947): The dynamics of long waves in a baroclinic westerly current, *J. Meteor.*, **4**, 135-163.

EADY, E.T. (1949): Long waves and cyclone waves, *Tellus*, **1**, 33-52.

GALL, R.L. (1976): A comparison of linear baroclinic instability theory with the eddy statistics of a general circulation model, *J. Atmos. Sci.*, **33**, 349-373.

HANSEN, A., A. SUTERA and D.E. VENNE (1989): An examination of mid-latitude power spectra: evidence for standing variance and the signature of El Niño, *Tellus*, **41A**, 371-384.

HAYASHI, Y. (1971): A generalized method of resolving disturbances into progressive and retrogressive waves by space-Fourier and time cross-spectral analysis, *J. Meteor. Soc. Japan*, **49**, 125-128.

HELD, I.M. and A.Y. HOU (1980): Nonlinear axially symmetric circulations in a nearly inviscid atmosphere, *J. Atmos. Sci.*, **37**, 515-533.

JAPAN METEREOLOGICAL AGENCY, MARINE DEPARTMENT (1991): *Climate Charts of Sea Surface Temperatures of the Western North Pacific and the Global Ocean*, pp. 51.

MECHOSO, C.R., A. KITOH, S. MOORTHI and A. ARAKAWA (1987): Numerical simulations of the atmospheric response to sea surface temperature anomaly over the equatorial Eastern Pacific ocean, *Mon. Wea. Rev.*, **115**, 2936-2956.

PEDLOSKY, J. (1979): *Geophysical Fluid Dynamics* (Springer), pp. 624.

SCHNEIDER, E.K. and R.S. LINDZEN (1977): Axially symmetric steady state models of the basic state for instability and climate studies. Part I: linearized calculations, *J. Atmos. Sci.*, **34**, 263-279.

SPERANZA, A. and P. MALGUZZI (1988): The statistical properties of a zonal jet in a baroclinic atmosphere: A semilinear approach. Part I: two-layer, quasi-geostrophic model atmosphere, *J. Atmos. Sci.*, **45**, 3046-3061.

(received September 30, 1996;
accepted February 24, 1997)